

## RESEARCH ARTICLE

# *Admp* regulates tail bending by controlling ventral epidermal cell polarity via phosphorylated myosin localization in *Ciona*

Yuki S. Kogure<sup>1</sup>, Hiromochi Muraoka<sup>1</sup>, Wataru C. Koizumi<sup>1</sup>, Raphaël Gelin-alessi<sup>1</sup>, Benoit Godard<sup>2</sup>, Kotaro Oka<sup>1,3,4</sup>, Carl-Philipp Heisenberg<sup>2,\*</sup> and Kohji Hotta<sup>1,\*</sup>

## ABSTRACT

Ventral tail bending, which is transient but pronounced, is found in many chordate embryos and constitutes an interesting model of how tissue interactions control embryo shape. Here, we identify one key upstream regulator of ventral tail bending in embryos of the ascidian *Ciona*. We show that during the early tailbud stages, ventral epidermal cells exhibit a boat-shaped morphology (boat cell) with a narrow apical surface where phosphorylated myosin light chain (pMLC) accumulates. We further show that interfering with the function of the BMP ligand *Admp* led to pMLC localizing to the basal instead of the apical side of ventral epidermal cells and a reduced number of boat cells. Finally, we show that cutting ventral epidermal midline cells at their apex using an ultraviolet laser relaxed ventral tail bending. Based on these results, we propose a previously unreported function for *Admp* in localizing pMLC to the apical side of ventral epidermal cells, which causes the tail to bend ventrally by resisting antero-posterior notochord extension at the ventral side of the tail.

**KEY WORDS:** Tunicate, Tail bending, Intercalation, Polarity, Boat cell, Embryo shape

## INTRODUCTION

Although chordates display diverse shapes and sizes in the adult stage, they have similar shapes during the organogenesis period, called the phylotypic stage (Klaus, 1983). During the phylotypic stage, chordates pass through neurulation and subsequently reach the tailbud stage. At the chordate tailbud stage, the embryo tail elongates along the anterior-posterior (AP) axis, and most tailbud embryos become curved with their tail bending ventrally (Richardson et al., 1997).

The ascidian tunicate *Ciona intestinalis* type A (*Ciona robusta*) embryo also shows a curved body shape with its tail bending ventrally (ventroflexion) during the early- to mid-tailbud stages (stage 19 to stage 22, as defined by Hotta et al., 2007), after which bending relaxes again, and eventually the tail bends dorsally

(dorsiflexion). This dynamic body shape change occurs even if the egg envelope is removed, suggesting that *Ciona* tail bending can occur in the absence of external spatial confinement (Hotta et al., 2007; Nakamura et al., 2012; Matsumura et al., 2020; Lu et al., 2020).

During tail extension, notochord cells change their shape by circumferential contraction between stages 21 and 24 (Lu et al., 2019; Mizotani et al., 2018; Sehring et al., 2014). This circumferential contraction, when applied on a compression-resisting system, such as the notochord, is converted into a pushing force along the AP axis of the notochord, thereby elongating the notochord (Lu et al., 2019; Miyamoto and Crowther, 1985).

Although it has been shown that an AP pushing force is exerted by each notochord cell (Sehring et al., 2014; Zhou et al., 2015) and that tail elongation is achieved by the notochord actively producing AP elongating forces (Miyamoto and Crowther, 1985; Sehring et al., 2014; Spemann, 1987; Ubisch, 1939), the mechanism by which the tail bends in the tailbud-stage embryo is only incompletely understood. Recently, Lu et al. (2020) have shown that tail bending in *Ciona* during the early tailbud stages (stages 18 to 20) is caused by the actomyosin cytoskeleton displaying contraction forces that are different at the ventral side compared with the dorsal side of the notochord. However, the upstream regulators involved in *Ciona* tail bending and the morphogenetic mechanisms driving tail bending after stage 20 remain unclear.

In this study, we used a combination of genetic, cell biological and biophysical/three-dimensional (3D) imaging experiments to show that *Admp* regulates cell polarity by determining the localization of phosphorylated myosin light chain (pMLC) at the apex of ventral midline epidermal cells. This ventral epidermal myosin accumulation leads to ventral tail bending by resisting notochord-driven AP tail elongation specifically at the ventral side during mid-tailbud stages.

## RESULTS


### *Admp* is required for ventral but not dorsal tail bending

Previous studies about *Admp* function did not focus on tail bending but the phenotype was apparent in their images. The knockdown of *Admp* has been shown to cause reduced ventral tail bending in mid-tailbud-stage *Ciona* embryos (Imai et al., 2006; Imai et al., 2012; Pasini et al., 2006). As these studies did not focus on the tail-bending morphant phenotype, we decided to mechanistically dissect how *Admp* functions in ventral tail bending.

To confirm that *Admp* is indeed required for *Ciona* ventral tail bending, we first performed microinjection of *Admp* morpholinos (MOs) and observed the morphant phenotype by recording time-lapse movies (Fig. 1A; Movie 1). We found that ventral tail bending (ventroflexion; Fig. 1A, red arrow) did not occur in *Admp* morphant embryos at the mid-tailbud stages; in contrast, dorsal tail bending (dorsiflexion; Fig. 1A, yellow arrows) was unaffected in morphant embryos. Comparison of the bending angle of *Admp* morphant with wild-type (WT) embryos from stage 18 to stage 22, when

<sup>1</sup>Department of Biosciences and Informatics, Faculty of Science and Technology, Keio University, Kouhoku-ku, Yokohama 223-8522, Japan. <sup>2</sup>Institute of Science and Technology Austria, Klosterneuburg, 3400, Austria. <sup>3</sup>Waseda Research Institute for Science and Engineering, Waseda University, 2-2 Wakamatsucho, Shinjuku, Tokyo 162-8480, Japan. <sup>4</sup>Graduate Institute of Medicine, College of Medicine, Kaohsiung Medical University, Kaohsiung City 80708, Taiwan.

\*Authors for correspondence (khotta@bio.keio.ac.jp; heisenberg@ist.ac.at)

 Y.S.K., 0000-0002-4802-5579; B.G., 0000-0003-4767-2915; C.-P.H., 0000-0002-0912-4566; K.H., 0000-0003-4614-7473

This is an Open Access article distributed under the terms of the Creative Commons Attribution License (<https://creativecommons.org/licenses/by/4.0>), which permits unrestricted use, distribution and reproduction in any medium provided that the original work is properly attributed.

Handling Editor: Thomas Lecuit

Received 21 September 2021; Accepted 12 September 2022

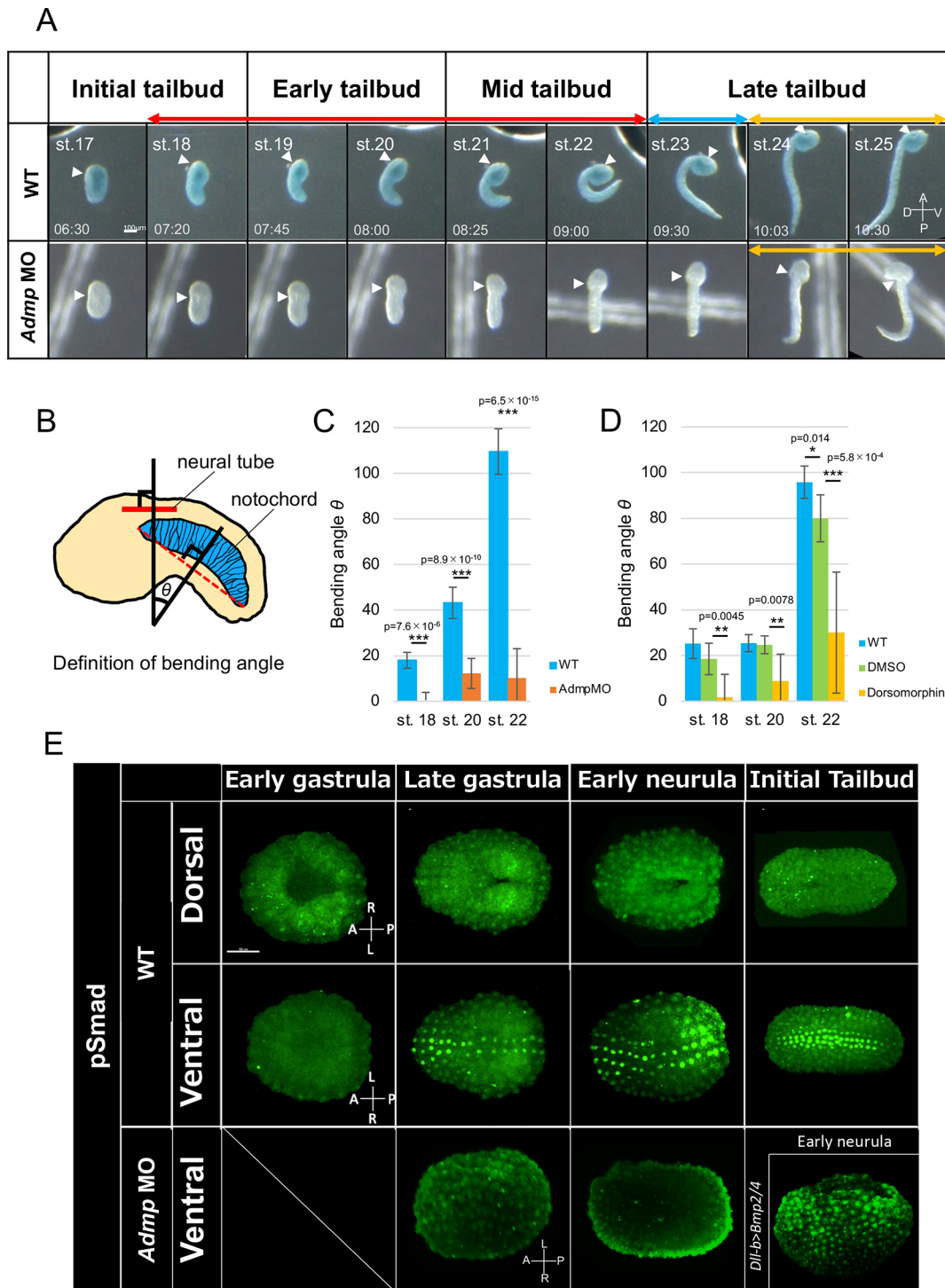


**Fig. 1. *Admp* affects the tail bending of early tailbud-stage embryos and pSmad is detected at the ventral midline epidermis.** (A) Images from a time-lapse movie of WT and *Admp* MO embryos ( $n=6/6$ ). WT and *Admp* MO embryos were developed in the same dish, and WT embryos were stained by Nile Blue B to distinguish them as previously described by Matsumura et al. (2020). Note that *Admp* MO suppressed ventral tail bending (ventroflexion) during early- to mid-tailbud stages (red double-headed arrow) but not dorsal tail bending (dorsiflexion) during the late tailbud stage (yellow double-headed arrow) after ‘relaxation’ (blue double-headed arrow) at the beginning of late tailbud stage. The developmental stage and time (hh:mm) after fertilization are shown in each WT picture. White arrowheads indicate the position of the neuropore. Scale bar: 100  $\mu$ m. A, anterior; P, posterior; D, dorsal; V, ventral. (B) The bending angle of the embryo tail was defined as the intersection angle of the straight line perpendicular to the neural tube of the trunk (solid red line) and the anterior-posterior border of the notochord cell (dashed red line), which is the 20th counting from an anterior-most notochord cell. (C) Quantification of the bending angle  $\theta$  of WT ( $n=8$ ) and *Admp* MO ( $n=5-15$ ) embryos at stages 18, 20 and 22. The bending angle was significantly reduced in *Admp* MO embryos. (D) Quantification of the bending angle  $\theta$  of WT ( $n=8$ ), DMSO-treated embryos ( $n=6-7$ ) and dorsomorphin-treated embryos ( $n=9-12$ ). The bending angle was significantly reduced in dorsomorphin-treated embryos. Data in C,D are mean  $\pm$  s.d. Two-tailed, unpaired *t*-test was used to determine significance. (E) Antibody staining against phosphorylated Smad1/5/8 (green), indicating *Admp*/BMP signaling, which was detected from the late gastrula at ventral midline cells in WT embryos. However, no signals were detected in *Admp*-MO. Ectopic signals were detected at the whole epidermal cells in the *Dll-b>Bmp2/4* embryo (right bottom panel). Images are representative of two embryos for each stage. Scale bar: 50  $\mu$ m.

ventroflexion occurs in WT (Fig. 1B), showed that the degree of ventroflexion was significantly reduced in morphant embryos (Fig. 1C;  $N=11/11$ ). Likewise, embryos treated with dorsomorphin, an Admp/BMP signaling inhibitor, also displayed a significantly reduced ventral tail bending angle ( $n=5-12$ , Fig. 1D; Fig. S1A,B). Taken together, these experiments indicate that Admp/BMP signaling regulates the ventroflexion of ascidian tailbud embryos.

Admp is a BMP ligand, which, in *Ciona*, has been reported to induce the differentiation of ventral peripheral neurons (Imai et al., 2012; Waki et al., 2015), with the homeobox gene *Mxsb* functioning as a downstream effector of Admp signaling in this process (Imai et al., 2012). We thus investigated whether *Mxsb* might also function as a downstream effector of Admp signaling in *Ciona* ventroflexion. However, ventroflexion appeared normal in *Mxsb* morphant embryos (Fig. S1C), suggesting that *Mxsb*, does not function as a downstream effector of Admp signaling in ventroflexion, unlike in neuronal differentiation (Roure and Darras, 2016; Waki et al., 2015).

### Smad phosphorylation in ventral midline epidermal cells

In *Ciona*, *Admp* is expressed in the endoderm and lateral epidermis (Imai et al., 2012). In vertebrates, *Admp* is first expressed dorsally within the embryo, and then Admp protein physically moves to the opposite side to specify the ventral fate, but it is difficult to predict the site of Admp activity from its gene expression pattern. Moreover, *Admp* promotes *bmp4* expression and controls the positioning of *bmp4* expression during regeneration of left-right asymmetric fragments in planarians (Gaviño and Reddien, 2011).

In *Ciona*, *Admp* expression appears normal in *Bmp2/4* morphants, but *Bmp2/4* expression is suppressed in *Admp* morphants (Imai et al., 2012). Furthermore, the BMP target Smad is phosphorylated by Admp signaling, followed by translocation of phosphorylated Smad into the nucleus and activation of target genes (Blitz and Cho, 2009; De Robertis, 2009; Imai et al., 2012). In line with this, Smad phosphorylation and activation in ventral epidermal cells is reduced in *Ciona Admp* morphants at the late gastrula stage (Fig. 1E; Waki et al., 2015).

To determine when and where within the tailbud stages *Ciona* embryo Admp/BMP signaling is activated, we performed antibody staining of phosphorylated pSmad1/5/8 (Fig. 1E). Consistent with a previous study (Waki et al., 2015), pSmad staining was observed in ventral midline epidermal cells after the late gastrula stage (Fig. 1E), whereas no specific signal was detected in other regions, including the notochord, from the gastrula to the initial tailbud period. This indicates that Admp/BMP signaling is specifically activated in ventral midline epidermal cells.

Asymmetric activation of actomyosin contractility in notochord cells has recently been proposed to be responsible for ventroflexion between stages 18 and 20 (Lu et al., 2020). To test whether Admp functions in ventroflexion by affecting asymmetric actomyosin contraction within notochord cells, we analyzed actin localization in Admp signaling-defective embryos. We found that in both dorsomorphin-treated and *Admp* morphant embryos, asymmetric actin localization in notochord cells remained unchanged (Fig. S2). This indicates that Admp/BMP signaling affects ventroflexion independently of the proposed function of asymmetric actomyosin contraction in notochord cells.

### Admp is required for ordered cell-cell intercalation of ventral epidermal cells

Next, we investigated the dynamics of dorsal and ventral epidermal cell rearrangements during ventral tail bending from stage 18 to

stage 24 (Fig. S3). Cell-cell intercalation of ventral epidermal cells started at stage 19 and was completed by stage 24. The tail epidermis of the ascidian embryo completes elongation along the AP axis by arranging epidermal cells in a row along this axis through cell-cell intercalation (Fig. S3; Hotta et al., 2007). Interestingly, in the period between stages 19 and 22, which reflects the early phase of epidermal cell-cell intercalation when ventroflexion occurs, intercalation was not associated by AP elongation of the ventral tail, whereas during later stages of epidermal cell-cell intercalation (stage 22 to stage 24), intercalation was accompanied by ventral tail elongation (Fig. 2A,B). We thus hypothesized that epidermal cell dynamics during the early intercalation period contribute to ventroflexion. To test this hypothesis, we compared epidermal cell dynamics between WT and ventroflexion-deficient *Admp* morphant embryos.

Between stages 20 and 22, the ventral epidermis in WT embryos showed a preferential accumulation of junctional F-actin in the medio-lateral (ML) direction (ML accumulation) (Fig. 2C). Antibody staining of pMLC also showed such ML accumulation, especially from stage 19 to stage 22 (Fig. S4). In contrast, no such ML accumulation was observed in *Admp* morphant embryos between stages 20 and 22 (Fig. 2C). In addition, although the AP/ML aspect ratio of ventral epidermal cells decreased in WT embryos from stage 18 to stage 22, no such decrease was found in *Admp* morphants (Fig. 2D). This suggests that *Admp* is required for proper asymmetric junctional actin accumulation and ML elongation of ventral epidermal cells during early intercalation. At stage 24, the tail epidermis in WT embryos became organized into eight distinct single-cell rows as a result of cell-cell intercalations (Fig. 2E,F) (Hotta et al., 2007; Pasini et al., 2006). Moreover, these eight rows, consisting of three rows of dorsal, two rows of lateral, and three rows of ventral epidermal cells, were closely aligned (Fig. 2F, WT). In contrast, the ventral epidermal cells in *Admp* morphant embryos were disorganized into one or two rows, making it difficult to clearly distinguish between midline and medio-lateral cells (Fig. 2F, *Admp* MO; orange/red color). Dorsomorphin-treated embryos showed a similarly disordered ventral midline intercalation phenotype (Fig. S5), further supporting the notion that *Admp* regulates ordered ventral epidermal cell-cell intercalation.

### Ventral epidermal cells display a boat-like morphology during ventroflexion

We suspected that defective ventroflexion in *Admp* morphant embryos involves changes in ventral epidermal cell morphologies (Fig. 2F). To further investigate in detail the morphological change that occurs in the ventral epidermal cells during this period, we monitored changes in single ventral epidermal cell morphology by 3D imaging. This revealed that ventral epidermal cells acquire a distinctive boat-like morphology (boat cell, Fig. S6), characterized by a larger area on the basal surface (Fig. 3A,B, yellow areas) compared with the apical surface (Fig. 3A,B, red areas), and ridges at both ends oriented along the ML direction. Almost all anterior ventral epidermal cells showed this shape (Movie 2), consistent with previous reports that tail bending only occurs in the anterior tail of *Ciona* (Lu et al., 2020). The shape of boat cells is characterized by a triangular cross-section where the apical surface is entirely constricted (triangular section of boat cell, TSBC), and a square cross-section where some apical surface is left (square section of boat cell, SSBC) (Fig. 3A,B). In *Admp* morphant embryos at stage 22, the number of TSBCs in ventral epidermal cells was strongly reduced (Fig. 3D,E; *Admp* MO,  $n=12$ ; WT,  $n=7$ ;  $P=0.05 \times 10^{-5}$ , two-tailed, unpaired Student's *t*-test), whereas the number of square

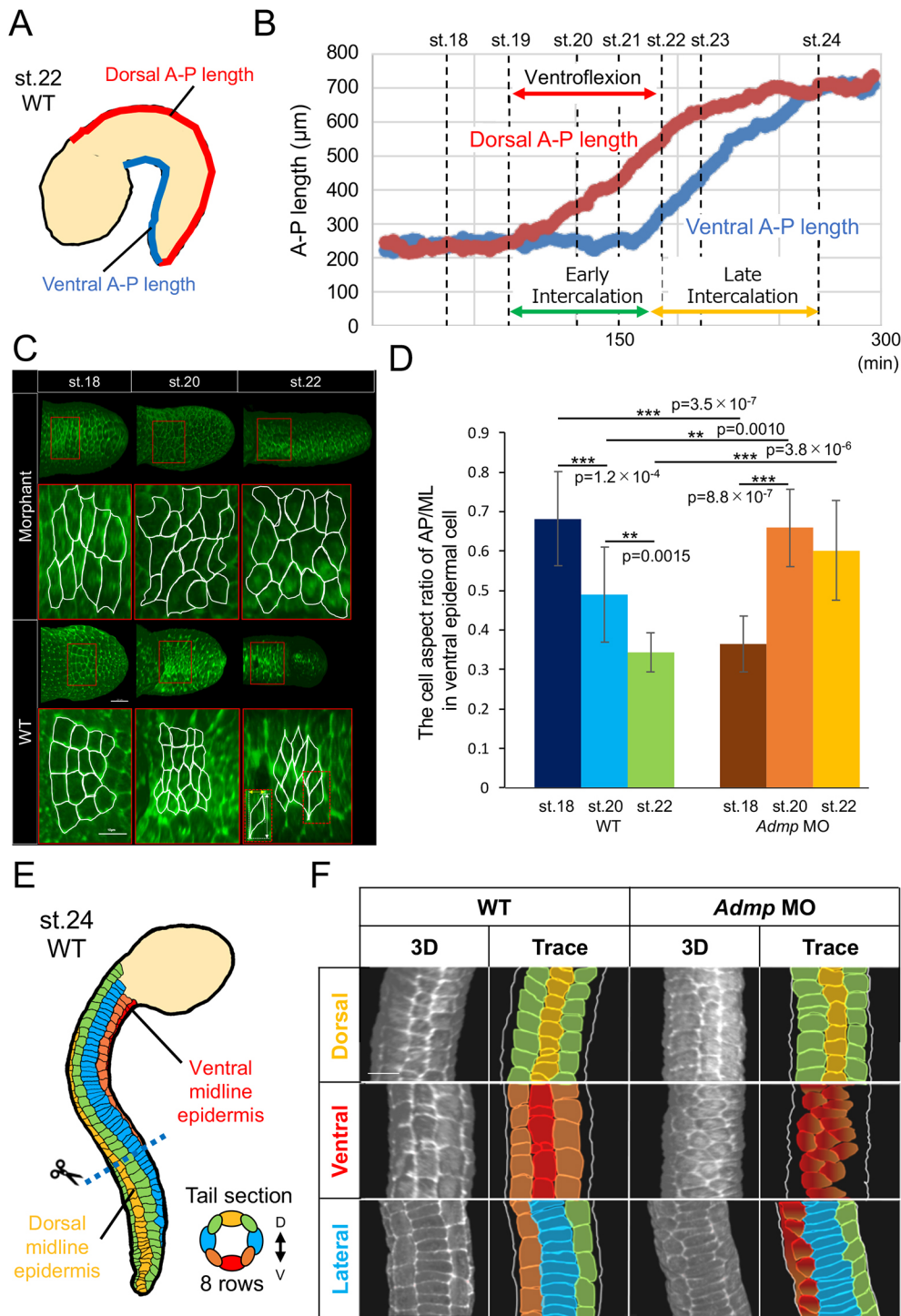


**Fig. 2. Comparison of the phenotypes of *Admp* MO and WT embryos.** (A) Schematic indicating the measurement of the tail length on the dorsal side (red line) and the ventral side (blue line). (B) Time-course measurements of the lengths of the dorsal outline (red line) and the tail region's ventral outline (blue line). Dorsal AP length of the tail epidermis (red) increases earlier than that of ventral AP (blue). The ventral AP length does not change during early intercalation (red double-headed arrow), indicating that the gap between them increases in this period. The ventral AP length increased at late intercalation (yellow double-headed arrow) and the gap decreased. Each black dotted line indicates the corresponding developmental *Ciona* stage. At stage 24, the dorsal AP and ventral AP outlines have the same length. Data are representative of one individual. (C) The changes in cell shape of anterior ventral epidermis of WT and *Admp* morphants during early intercalation, which were stained for F-actin by phalloidin. The figures show the ventral view and the cell shapes were traced with white lines. In all figures, the anterior ventral tail epidermal cells were perpendicular to the direction of observation. Scale bars: 20  $\mu$ m. (D) The AP/ML aspect ratio of the ventral epidermis of WT and *Admp* morphants during early intercalation as seen in C was measured with reference to the ratio between ML length and AP length in each cell as shown in the red dotted rectangle in C (WT: stage18,  $n=14$ ; stage 20,  $n=19$ ; stage 22,  $n=10$ . *Admp* MO: stage18  $n=10$ ; stage 20,  $n=16$ ; stage 22,  $n=16$ ). Asterisks indicate statistical significance (two-tailed, unpaired *t*-test). The error bars indicate s.d. (E) The schematic alignment of the tail epidermal cells of WT embryos at stage 24. Cell-cell intercalation of the tail epidermis finishes by stage 24. The tail epidermal cells consist of eight rows: dorsal (yellow), two dorsal medio-lateral (green), ventral (red), two ventral medio-lateral (orange) and two lateral (blue) rows. The blue dotted line indicates the location of tail cross-section drawing on the right. (F) The alignment of the tail epidermal cells of WT and *Admp* MO embryos at stage 24. There is a specific inhibition of the intercalation of the ventral rows (red and orange) in *Admp* MO embryos ( $n=4$  in WT and  $n=4$  in *Admp* MO). The mixed colors indicate that we were unable to distinguish ventral and ventrolateral epidermal cells. Scale bar: 10  $\mu$ m.

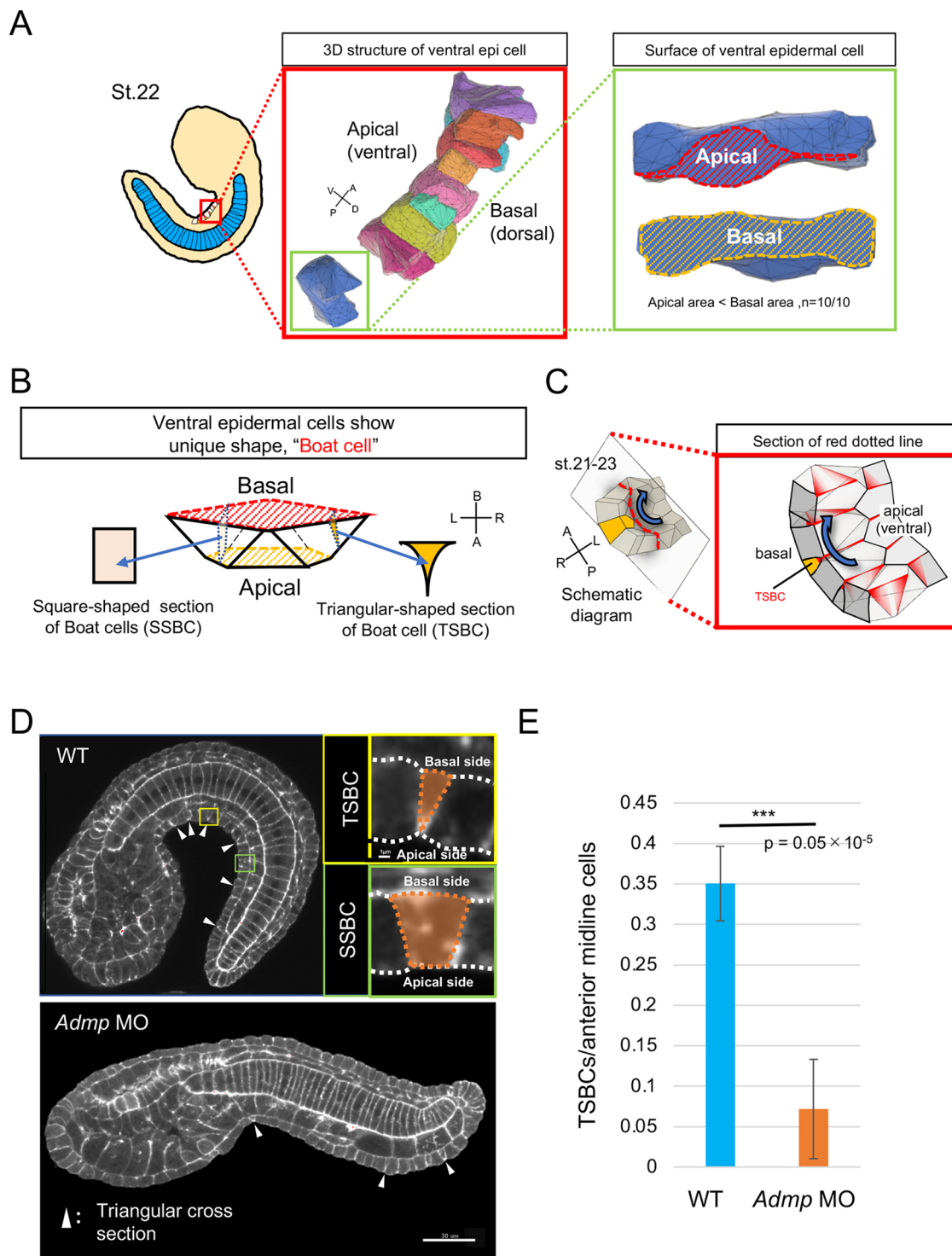


**Fig. 3. 3D reconstruction of ventral midline epidermal cells during tail bending.** (A) 3D model reflecting the shape of each midline ventral epidermal cell at stage 22 was reconstructed using Avizo6 software (red boxes) as described by Matsumura et al. (2020). Representative morphology of ventral midline cells is shown (green boxes). Each cell is bipolar laterally and has protrusions from basal parts. Note that the apical area (red) is smaller than the basal area (yellow). (B) The 3D model reflects the shape of ventral epidermal cells in A. The ventral epidermal cells show a distinctive boat-like shape. The sections of the boat cell show triangular (TSBC) or square (SSBC) shapes depending on the plane. (C) Schematic of the cell-cell intercalation of the ventral midline epidermal cells using boat cells during the tail-bending period. The ventral midline epidermis consists of boat cells with a smaller apical domain area than the basal domain; leading to overall bending of the tissue (blue arrow). The midline section of the orange cell (cut in the red dotted plane) shows a TSBC. The orange cell starts intrusion from basolateral sides with pMLC protrusions (red colored). The 3D models were generated manually by FUSION 360 educational version (Autodesk; <https://www.autodesk.co.jp/campaigns/education/fusion-360>). (D) Midline section view of WT tailbud embryo and *Admp* MO embryo at stage 22 by staining of F-actin. Arrowheads indicate the position of TSBCs. The magnified views of the yellow and green boxes show a TSBC and a SSBC, respectively. Scale bar: 30  $\mu$ m. (E) The ratio of the number of TSBCs and the number of midline cells. It has been reported that the driving forces of the tail bending originate in the anterior part of the tail (Lu et al., 2020). Therefore, we counted the number of TSBCs in the anterior part of the tail. TSBCs were significantly reduced in *Admp* MO embryos. Asterisks indicate statistical significance (two-tailed, unpaired *t*-test). The error bars indicate s.d. (WT,  $n=8$ ; *Admp* MO,  $n=6$ ).

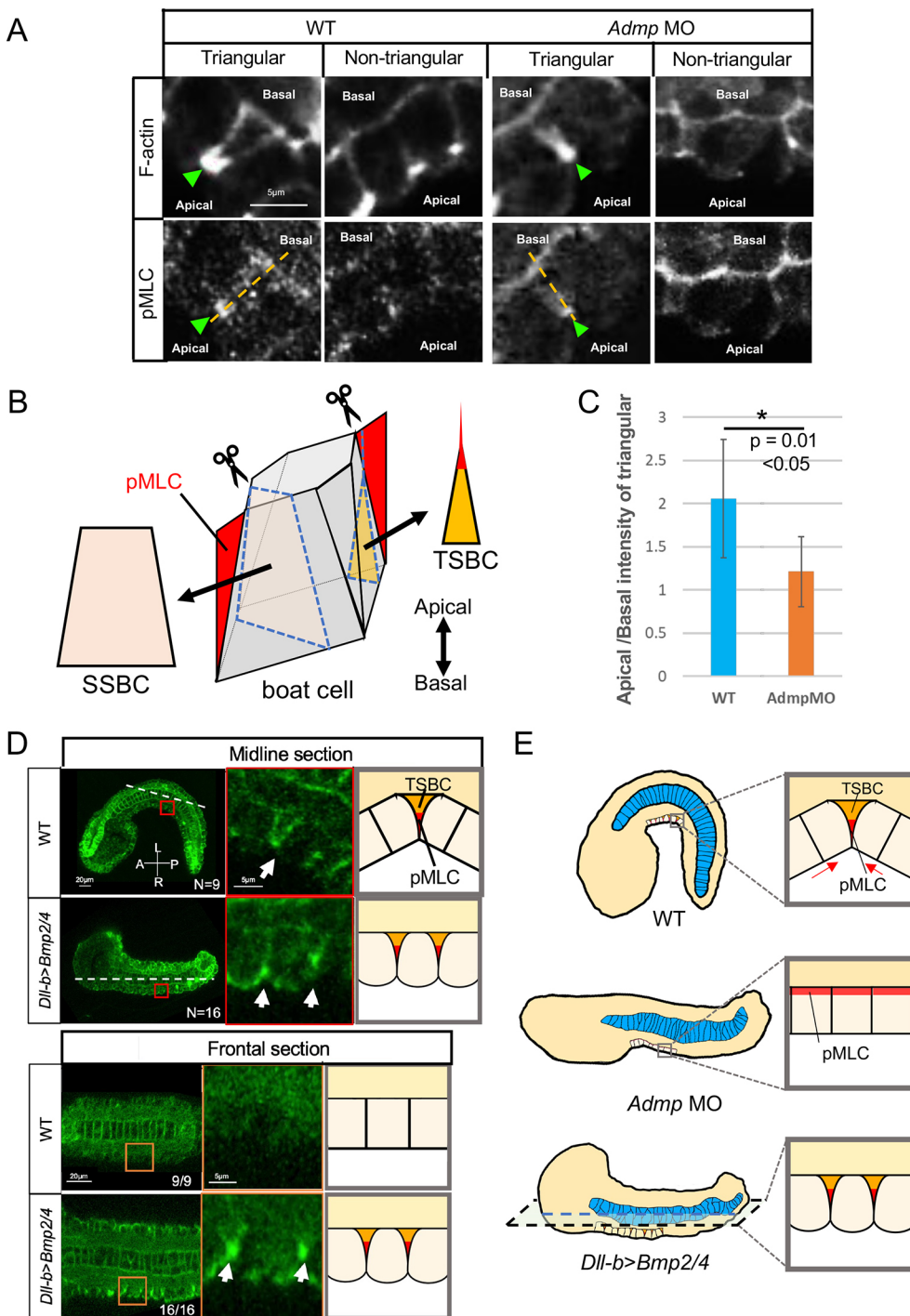


**Fig. 4. The distribution of pMLC in the tail epidermis depends on the *Admp*/BMP signaling pathway.** (A) Double staining of F-actin and phosphorylated myosin light chain (pMLC) of the ventral midline of WT and *Admp* MO embryos at stage 22. Both F-actin and pMLC accumulated at the apical side of triangular cells (green arrowheads). The loci of the measurements for the relative pMLC intensity between the apical and basal side of the epidermis in WT and *Admp* MO embryos are shown as yellow lines. Scale bar: 5  $\mu$ m. (B) The 3D model of a boat cell reflecting the localization of pMLC (red). Different section planes show different shapes: triangular (TSBC) and square (SSBC). (C) Relative pMLC intensity between the apical and basal side of the epidermis in WT ( $n=10$  cells from 10 embryos) and *Admp* MO ( $n=7$  cells from 7 embryos). Asterisk indicates statistical significance (two-tailed, unpaired *t*-test). The error bars indicate s.d. (D) The distribution of pMLC in WT and *Dll-b>Bmp2/4* at stage 22. In the midline section, pMLC was distributed at the apical TSBCs of the ventral midline epidermis in both WT and *Dll-b>Bmp2/4* (arrows in the red boxes). However, in the frontal section, the apical TSBCs of the lateral epidermis were observed in *Dll-b>Bmp2/4* embryo (arrows inside the orange rectangle), but there was no pMLC signal in the lateral epidermis in WT. The white dashed lines indicate the section plane of the frontal sections. (E) Schematic of the difference in the distribution of pMLC (red) among WT, *Admp* MO and *Dll-b>Bmp2/4* embryos. The orange-colored cell sections are TSBCs.

sections of cells that were not boat cells was increased, indicative of a reduced number of boat cells in all ventral epidermis sections of morphant embryos (Movie 2).

#### ***Admp*/BMP signaling is required for the localization of the pMLC to the apical side of ventral epidermal cells**

To understand how this distinctive boat-cell morphology (Fig. 3A, B) arises, we performed both F-actin/phalloidin staining and antibody staining for pMLC. This showed an accumulation of both F-actin and pMLC at the apical side of TSBCs (Fig. 4A,B, WT arrowheads). Interestingly, the localization of pMLC to the apical side was significantly decreased in *Admp* morphant embryos

(Fig. 4C; *Admp* MO,  $n=7$ ; WT,  $n=9$ ;  $P=0.01$ , two-tailed, unpaired Student's *t*-test), suggesting that *Admp* triggers the formation of TSBCs, and thus boat-cell shape, by localizing pMLC to the apical side of ventral midline cells.

To test whether *Admp*/BMP signaling can ectopically affect the localization of pMLC and thereby generate TSBCs (Fig. 4D), we performed ectopic *Bmp* expression experiments. In WT embryos, apical pMLC accumulation and TSBCs were not observed in epidermal cells, except in ventral epidermal cells, where pSmad signal was also detected (Fig. 4D, frontal section of WT). In contrast, in embryos ectopically expressing BMP, pSmad signal was detected in all epidermal cells, accompanied by apical pMLC

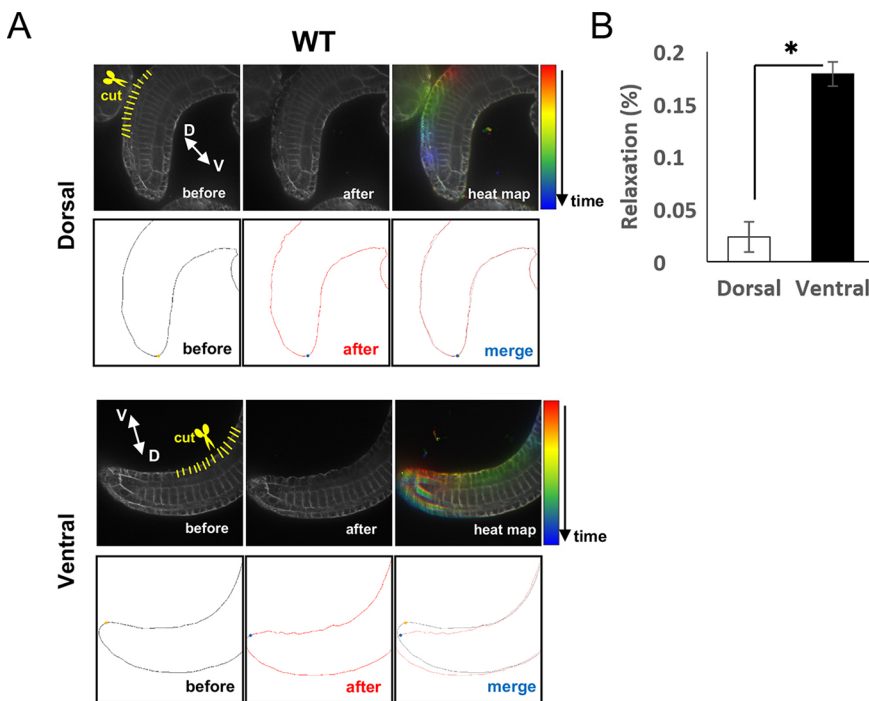


**Fig. 5. Laser cutting experiment for the AP cell-cell border of the tail epidermis.** (A) Laser cutting of the WT dorsal and ventral midline epidermis at stage 22. Epidermal cells are a monolayer. We cut each cell in an apicobasal direction (yellow lines). Cell membranes were stained by FM4-64. The color bar indicates the time after laser cut from 0 s (before) to 30 s post cut. (B) The movement of the area before and after the laser cut was calculated as relaxation ( $n=5$ ). Asterisk indicates statistical significance (two-tailed, unpaired  $t$ -test,  $*P<0.05$ ). The error bar indicates s.d.

accumulation and TSBC formation not only in ventral tail epidermal cells but also within the remainder of the tail epidermis (Fig. 4D).

This suggests that *Admp*/BMP signaling is sufficient to induce the localization of pMLC to the apical side of epidermal cells (Fig. 4E), leading to the formation of boat cells. This cell-shape change, again, might resist tail elongation at the ventral tail region, leading to ventroflexion.

#### Cutting ventral epidermal cells relaxes ventroflexion

To investigate whether the ventral epidermis indeed locally resists tail elongation, eventually leading to ventroflexion, we cut either ventral or dorsal epidermal cells at their apex along the AP axis using an ultraviolet (UV) laser cutter (Fig. 5, yellow lines). When dorsal midline epidermal cells were cut, no effect was observed. However, cutting ventral midline epidermal cells led to a strong relaxation of ventroflexion, indicative of stress release along the AP axis at ventral midline epidermal cells (Fig. 5A,B; Movie 3). These findings suggest that apically accumulated pMLC in boat cells generate AP stress in the ventral midline epidermis, resisting tail elongation and thus enabling ventroflexion.

We further investigated whether the relaxation of ventroflexion by UV laser cutting depends on whether the cuts were oriented along the AP axis or ML axis in ventral midline cells. This showed that the relaxation of ventroflexion was slower in AP cuts compared with ML cuts (Movie 4), consistent with the notion that ML cuts more efficiently interfere with AP stress in the ventral epidermis midline than AP cuts.

#### pMLC localization predicts development of boat-cell morphology

Next, we asked how boat cells change their shape during the ventral tailbud period (Fig. 6A). To this end, we analyzed the subcellular distribution of pMLC as a proxy for actomyosin contraction in ventral midline cells (ventral view in Fig. S4). This revealed that pMLC first emerged at the ML junction of ventral midline epidermal cells at stage 21 (Fig. 6A, stage 21 arrowheads) and localized to the apical side of TSBCs at stage 22 (Fig. 6A, stage 22

arrowheads). At stage 23, the trapezoid shape became apparent at the midline plane (Fig. 6, stage 23; Fig. S4) and, finally, the apical accumulation of pMLC disappeared at stage 24 (Fig. 6, stage 24; Fig. S4). These observations suggest that TSBC formation is driven by ML contraction. The ML-directed localization of pMLC and the cell shape change to a boat-like morphology correspond with ventroflexion, and pMLC disappearance and the cell shape change away from the boat-like morphology correspond with relaxation.

## DISCUSSION

### *Admp* is an upstream regulator of tail bending

Originally, the *Admp*/BMP pathway was identified to be central in establishing, maintaining and regenerating the dorsoventral axis among bilaterian animals (Gaviño and Reddien, 2011). In the ascidian, both gain- and loss-of-function experiments demonstrated that *Admp* expressed in the B-line medial vegetal cells acts as an endogenous inducer of the ventral epidermis midline (Pasini et al., 2006). *Admp* is required for sensory neuron differentiation of the ventral epidermis via expression of the *Tbx2/3* and *Msx* genes (Waki et al., 2015). Our finding that tail bending was not regulated by *Msx* (Fig. S1C) suggests that *Admp* functions in ascidian tail bending through different effector pathways than those implicated in ventral epidermal cell-fate specification. *Admp* controls ventral but not dorsal tail bending by determining early ventral epidermal cell intercalation (Fig. 2) and the shape of ventral epidermal midline cells (Fig. 3) through the localization of pMLC (Fig. 4). Importantly, this does not exclude the possibility that genes other than *Admp* act on tissues other than the ventral epidermis to control ventroflexion.

### *Admp* controls ordered cell-cell intercalation of ventral epidermal cells

We divided the intercalation period into two phases: during early intercalation, the ventral epidermis does not elongate in an AP direction; during late intercalation, in contrast, the ventral epidermis elongates. Interestingly, ventral tail bending (ventroflexion) occurs during early intercalation, with ventral epidermal cells displaying a

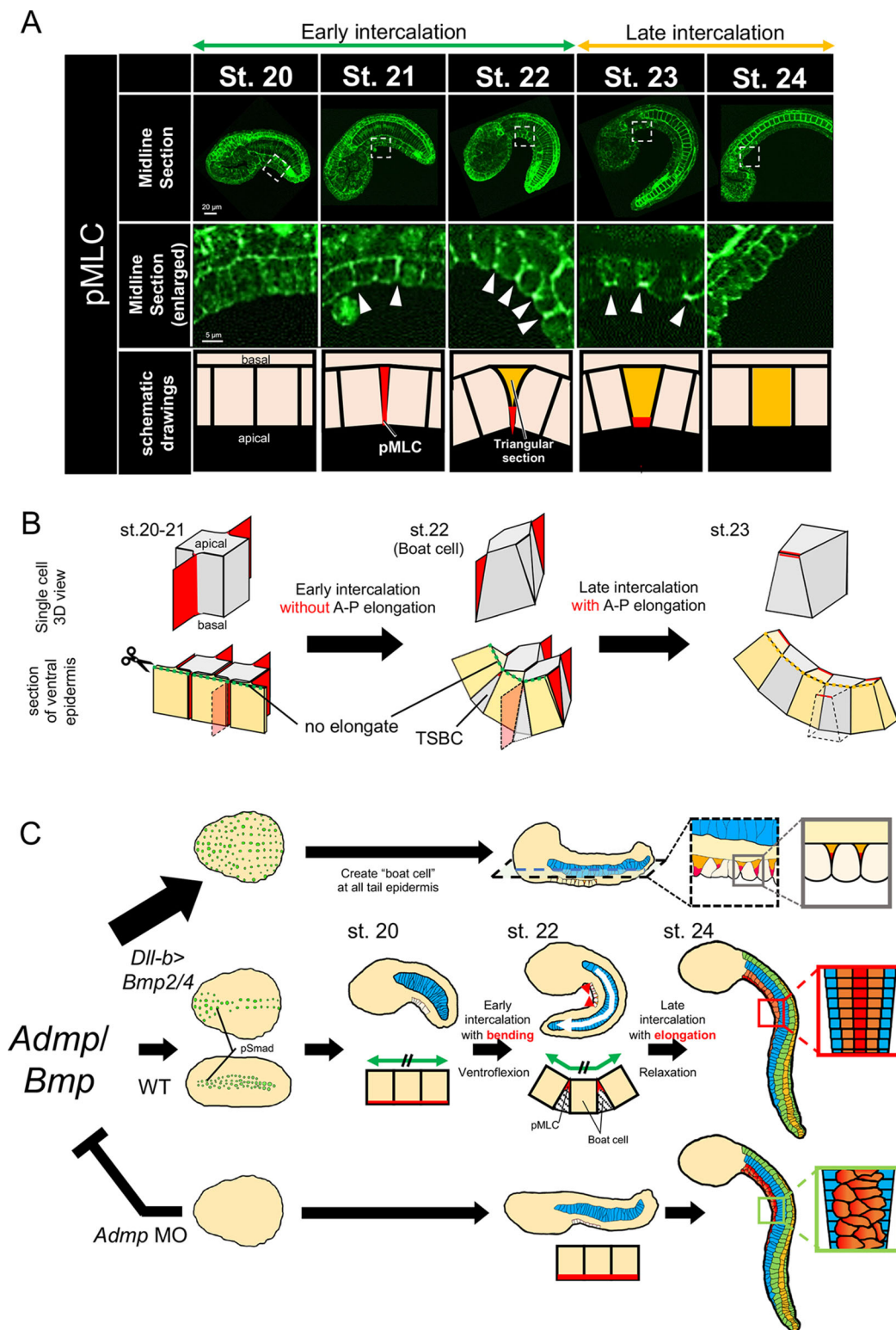


Fig. 6. See next page for legend.

flat shape elongated along the ML axis (Fig. 2C,D). We assume that this ML cell elongation is caused by the accumulation of actomyosin in ML-oriented protrusion-like extensions of ventral epidermal cells (Fig. 6B) that extend cells along the ML axis (Fig. S7). No such actomyosin localization and ML elongation was found in *Admp* morphant embryos, suggesting that *Admp* is required for ventral epidermal cell polarization and protrusion formation.

When ventral epidermal cell intercalation is completed (approximately by stage 24), ventral epidermal cells drastically change their polarity into the AP direction in WT embryos. This does not occur to the same extent in *Admp* morphants (Fig. 2D), suggesting that *Admp* is also required for this later shift in cell polarity.

Ventral tail epidermal cells in WT but not *Admp* morphant embryos arrange into three ordered rows at stage 24. This suggests



### Fig. 6. Relationship between the change of the distribution of pMLC and tail bending during intercalation of midline epidermal cells.

(A) Antibody staining of pMLC (top) from stage 20 to stage 24 in WT. Scale bar: 20  $\mu$ m. Enlarged views of the dotted rectangles in each stage (middle). Arrowheads show pMLC accumulation in the apical domain of the ventral midline epidermal cells. Schematics (bottom) of the distribution of pMLC (shown in red). At stage 20, pMLC localizes at the basal side of the epidermis. At stage 21, pMLC appears at the AP cell border of ventral midline epidermal cells. At stage 22, pMLC accumulates at the apex of the apical domain and the cell shape changes to triangular (boat cell shown in Fig. 3C) (orange-colored cell). pMLC localization at the basal side is reduced. At stage 23, the apex of the apical domain becomes broader. At stage 24, the pMLC asymmetrical distribution of pMLC disappears. (B) The schematic model explains the halt of AP elongation during the early intercalation period. At the beginning of the intercalation, the total AP length of the midline cells is shown as a dotted green line (stage 20). During early intercalation, the ventral epidermal cells change shape to become boat cells. The boat cells start to intrude on each other from the basal plane. Still, the total AP length of the apical side does not change (dotted green line) because apically accumulated pMLC (stage 22) resists the AP elongation force of the notochord. In late intercalation, the boat cell intercalates the basal and apical sides, and the apical area increases, allowing the elongation of AP length (dotted yellow line) of the apical side (stage 23). (C) Model of embryonic tail bending in *Ciona*. Admp/BMP signaling (green dots) transmits the signal to the ventral midline epidermal cells as phosphorylated Smad from the neurula to the initial tailbud. pSmad translocates the localization of the pMLC from the basal (dorsal) to the apical (ventral) side, which changes the cell polarity and promotes the cell-cell intercalation of the ventral midline epidermal cells during early- to mid-tailbud stages (stage 20 to stage 23). The ongoing mediolateral intercalation at the ventral epidermis confers a resistance (red arrowheads) to AP elongation force (white arrow) that is possibly provided by the notochord, which causes the bending in the *Ciona* tailbud embryo at stage 22. Conversely, the *Admp* MO or dorsomorphin treatment disrupts cell polarity and prevents tail bending in embryos at stages 20-23 and incomplete intercalation at stage 24 (green box). The final overall embryo shape at stage 24 is similar between WT and *Admp* MO embryos, but the ventral cell-cell intercalation is disrupted (red/orange cells). Thus, Admp/BMP signaling, apart from its known role in peripheral nervous system differentiation, regulates temporal tail bending during the early- to mid-tailbud stages (stage 20 to stage 23).

that *Admp* may be required for the cell autonomous ML intercalation of ventral epidermal cells by controlling ML cell polarization and protrusion formation. Notably, in *Admp* morphants, the ventral epidermis was disordered but kept a three-cell width, suggesting that some intercalation of ventral epidermal cells might still occur in the absence of *Admp*.

How does the intercalation of ventral midline cells contribute to ventroflexion? The ventral epidermis undergoing early cell intercalation does not elongate along the AP axis from stage 20 to stage 22, different from the already fully intercalated dorsal epidermis (Fig. 2B). Assuming that the notochord functions as the main force-generating structure driving tail elongation (Dong et al., 2011; Hara et al., 2013; Lu et al., 2019), the lack of ventral epidermis elongation between stages 20 and 22 might locally resist the global notochord-mediated tail elongation, thereby causing the tail to bend ventrally. The lack of ventral epidermis elongation along the AP direction during early intercalation is likely due to the *Admp*-dependent polarization of ventral epidermal cells along the ML direction. This cell polarization perpendicular to the AP direction can limit epidermal AP elongation during intercalation, which again, by resisting global notochord-driven tail elongation, leads to ventroflexion.

#### Admp regulates ventral epidermal cell-shape changes

Ventral epidermal cells take a distinct boat-like shape, which likely contributes to ventroflexion (Fig. 4; Fig. S7). The preferential

accumulation of pMLC in ventral epidermal cells along ML junctions (Fig. S4Db',Eb') is found at the apical side of cell boundaries of TSBCs and/or SSBCs and might correspond to protrusion-like extensions formed between interdigitating boat cells (Fig. 6B). The lack of such polarized distribution of pMLC suggests that *Admp* might be required for both planar and apicobasal polarization of these cells.

As the cell-cell intercalation of the boat cell progresses, the shape of these cells changes from a triangular to a trapezoidal shape (Fig. 6A). This shape change occurs during the late intercalation period (Fig. 2B) and leads to ventral epidermis elongation along the AP axis (Fig. 6B, green dotted line). Thus, ventral epidermal cell elongation along the ML axis during early intercalation locally resists notochord-mediated tail elongation, thereby triggering ventroflexion (Fig. 6B, stage 20 to stage 22). During later intercalation, in contrast, the ventral epidermal midline cells enlarge their apical area and elongate along the AP axis, thereby relaxing the local resistance against tail elongation (Fig. 6B, yellow dotted line, stage 23).

How does *Admp*/BMP signaling regulate both the cell-cell intercalation and the apicobasal polarity of the ventral epidermal cells? Our findings suggest that *Admp* is required for the preferential localization of pMLC not only at ML junctions between intercalating cells (Fig. S4), but also at the apical side by pSmad signaling (Fig. 4D). Recent studies show that SMAD3-driven cell intercalation underlies secondary neural tube formation in the mouse embryo (Gonzalez-Gobartt et al., 2021). Moreover, the BMP-Rho-ROCK1 pathway is thought to target myosin light chain to control actin remodeling in fibroblasts (Konstantinidis et al., 2011). Finally, BMP regulates cell adhesion during vertebrate neural tube closure and gastrulation (von der Hardt et al., 2007; Smith et al., 2021). Yet, how BMP/Smad signaling regulates the localization of pMLC in ventral epidermal cells is still unclear.

#### Model of ascidian ventroflexion

Our findings demonstrate that *Admp* is required for ventroflexion of the ascidian tail during tailbud stages (stages 18 to 22). We propose that *Admp* phosphorylates Smad in the ventral epidermis. pSmad, in turn, allows early cell intercalation within the ventral epidermis by controlling the localization of the pMLC, leading to ventral epidermal cells taking a boat-like shape. This cell-shape change limits ventral epidermal elongation along the AP axis, thereby locally resisting global notochord-driven tail elongation causing the tail to bend down (Fig. 6).

The notochord has recently been proposed to display asymmetric contraction forces before stage 20 by the asymmetrical localization of actomyosin in notochord cells (Lu et al., 2020). However, *Admp* morphant embryos displaying straight tails still have a ventral bias in notochord actomyosin localization (Fig. S2). This suggests that *Admp* is not required for asymmetrical notochord actomyosin localization, and that this asymmetric localization is not sufficient to cause ventroflexion. One possibility is that the ventral accumulation of actomyosin in the notochord might be involved in earlier morphogenetic events, such as notochordal cell intercalation, giving rise to a transient ventral groove (Munro and Odell, 2002).

#### The evolutionary roles of *Admp*

Our study provides insights into the molecular and mechanical mechanisms underlying conserved shape changes of chordate embryos, such as tail bending. Tail bending in tailbud-stage embryos is a still understudied morphogenetic process, even though

many genes, including *Admp*, with a crucial function in tail bending have been identified in zebrafish (Esterberg et al., 2008; Willot et al., 2002) and frog (Dosch and Niehrs, 2000; Kumano et al., 2006). In invertebrate non-chordate animals, such as sea urchins and hemichordates, *Admp* is expressed within the embryonic ectoderm (Chang et al., 2016; Lowe et al., 2006). It would thus be interesting to investigate whether the regulation of pMLC subcellular localization by *Admp* is conserved in primitive chordate embryogenesis and causes a change in body shape in these animals.

## MATERIALS AND METHODS

### Ascidian samples

*Ciona robusta* (*Ciona intestinalis* type A) adults were obtained from Maizuru Fisheries Research Station (Kyoto University, Japan), Onagawa Field Center (Tohoku University, Sendai, Japan) and Misaki Marine Biological Station (University of Tokyo, Japan) through the National Bio-Resource Project (Japan) and Roscof Marine Station (Roscof, France). Eggs were collected by dissection of the gonoducts. To distinguish WT and morphant embryos, embryos were stained with NileBlue B (Wako, Japan), which was gifted by Prof. Hiroki Nishida (Osaka University, Japan). After artificial insemination, fertilized eggs were incubated at 20°C until fixation or observation. Developmental stages followed Hotta's stages (Hotta et al., 2007, 2020). To inhibit phosphorylation of myosin, Y27632 (10 μM, Nacalai Tesque, Japan) was applied to embryos at 7 h post fertilization (late neurula, stage 16). Dorsomorphin (10 μM, Sigma-Aldrich) was applied to embryos after fertilization.

### Immunostaining and quantifying pMLC intensity

To detect activation of the *Admp*/BMP signaling pathway, we followed the same method described previously (Waki et al., 2015). To detect pSmad, we used a rabbit primary antibody (1/50, ab216482, abcam) and an Alexa Fluor 488-conjugated goat anti-rabbit secondary antibody from the Alexa Fluor 488 Tyramide SuperBoost Kit, (b40922, Invitrogen). The signal was visualized with a Tyramide Superboost Kit (Invitrogen) using horseradish peroxidase (HRP)-conjugated goat anti-rabbit IgG and Alexa Fluor 488 tyramide.

The method of pMLC antibody staining was as follows. Embryos were fixed in 3.7% formaldehyde in seawater for 30 min and then rinsed with PBS with 0.2% Triton X-100 (PBST) for 3 h. Embryos were incubated in PBST containing 10% goat serum for 3 h at room temperature or overnight at 4°C. Embryos were then incubated in the primary antibody (anti-rabbit Ser19 phosphorylated-1P-myosin, 1/50, 3671S, Cell Signaling Technology) diluted to 1:50 incubated for 3 h at room temperature or overnight at 4°C. The samples were then washed with PBST for 3 h. A poly-HRP secondary antibody (goat anti-rabbit IgG, Alexa Fluor 488, Tyramide SuperBoost Kit) was applied for 3 h and washed in PBST for 3 h. The Alexa Fluor dye tyramide (Alexa Fluor 488 Tyramide SuperBoost Kit) was added to the reaction buffer for 5-8 min to induce a chemical HRP reaction. Embryos were dehydrated through an isopropanol series and finally cleared using a 2:1 mixture of benzyl benzoate and benzyl alcohol.

pMLC accumulation was quantified by measuring the intensity along the ventral tail epidermis using Fiji image analysis software. The signal in the brain region was taken as the positive control because its signal was detected even in Y27632-treated embryos, indicating RhoA kinase (ROCK)-independent expression. The relative intensity of pMLC normalized to the intensity of the brain region in each individual was calculated by ImageJ for comparative analysis among different individuals.

### Laser cutting experiments

UV laser cutting experiments were performed on tailbud *Ciona* embryos. An inverted Axio Observer Z1 (Zeiss) microscope equipped with a confocal spinning disk (Andor Revolution Imaging System, Yokogawa CSU-X1), a Q-switched solid-state 355 nm UV-A laser (Powerchip, Teem Photonics), a C-APOCHROMAT 63×/1.2 W Korr UV-VIS-IR water immersion objective (Behrmdt et al., 2012) and a home-made cooling stage were used. The membranes of tail epidermal cells of tailbud embryos were labeled with FM-64 (Thermo Fisher Scientific). Each ventral midline

epidermal cell was cut along the apicobasal axis (5-10 μm lines each) by applying 25 UV pulses at 0.7 kHz. The embryos were imaged every 0.2 s with an exposure time of 150 ms. Single fluorescent images were used to measure tail relaxation 3 s post ablation, and the percentage of relaxation was calculated as the area of movement of the tail region 3 s after laser cutting.

### Gene knockdown and overexpression

The MOs (Gene Tools) against *Mxxb* and *Admp*, which block translation, were designed according to previous studies (Imai et al., 2006; Waki et al., 2015) and are as follows: *Admp*, 5'-TATCGTGTAGT TTGCTTTCTA-TATA-3'; *Mxxb*, 5'-ATTCGTTTACTGTCATTTTTAATTT-3'. These MOs were injected at 0.25-0.50 mM into an unfertilized egg and incubated until observation. To visualize the phenotype of *Admp* MO embryos at the single-cell level, embryos were stained using Alexa Fluor 546 phalloidin (1/50 diluted in PBS, A22283, Thermo Fisher Scientific) and imaged using an Olympus fv1000 microscope.

The DNA constructs used for overexpression of *bmp2/4* under the *Dlx.b* upstream sequence (Ciinte.REG.KH.C7.630497-632996|*Dlx.b*) were used previously (Imai et al., 2012). These DNA constructs were introduced by electroporation.

### Acknowledgements

*Ciona intestinalis* adults were provided by Dr Yutaka Satou (Kyoto University) and Dr Manabu Yoshida (the University of Tokyo) with support from the National Bio-Resource Project of AMED, Japan. We thank Dr Hidehiko Hashimoto and Dr Yuji Mizotani for technical information about 1P-myosin antibody staining. We thank Dr Kaoru Imai and Dr Yutaka Satou for valuable discussion about *Admp* and for the DNA construct of *Bmp2/4* under the *Dlx.b* upstream sequence. We thank Ms Maki Kogure for constructing the FUSION360 of the intercalating epidermal cell.

### Competing interests

The authors declare no competing or financial interests.

### Author contributions

Conceptualization: K.H.; Methodology: Y.S.K., W.C.K., R.G., B.G.; Software: R.G.; Validation: Y.S.K., W.C.K.; Formal analysis: Y.S.K., W.C.K.; Investigation: Y.S.K., H.M., W.C.K., R.G., B.G.; Resources: K.H., C.-P.H.; Data curation: Y.S.K., H.M., W.C.K., R.G.; Writing - original draft: Y.S.K., K.H.; Writing - review & editing: Y.S.K., K.O., C.-P.H., K.H.; Visualization: Y.S.K., W.C.K., H.M.; Supervision: B.G., K.O., C.-P.H., K.H.; Project administration: K.O., K.H.; Funding acquisition: K.H.

### Funding

This work was supported by funding from the Japan Society for the Promotion of Science (JP16H01451, JP21H00440). Open Access funding provided by Keio University: Keio Gijuku Daigaku. Deposited in PMC for immediate release.

### Peer review history

The peer review history is available online at <https://journals.biologists.com/dev/lookup/doi/10.1242/dev.200215.reviewer-comments.pdf>.

### References

- Behrmdt, M., Salbreux, G., Campinho, P., Hauschild, R., Oswald, F., Roensch, J., Grill, S. W. and Heisenberg, C. P. (2012). Forces driving epithelial spreading in zebrafish gastrulation. *Science* **338**, 257-260. doi:10.1126/science.1224143
- Blitz, I. L. and Cho, K. W. Y. (2009). Finding partners: how BMPs select their targets. *Dev. Dyn.* **238**, 1321-1331. doi:10.1002/dvdy.21984
- Chang, Y.-C., Pai, C.-Y., Chen, Y.-C., Ting, H.-C., Martinez, P., Telford, M. J., Yu, J.-K. and Su, Y.-H. (2016). Regulatory circuit rewiring and functional divergence of the duplicate *admp* genes in dorsoventral axial patterning. *Dev. Biol.* **410**, 108-118. doi:10.1016/j.ydbio.2015.12.015
- De Robertis, E. M. M. (2009). Spemann's organizer and the self-regulation of embryonic fields. *Mech. Dev.* **126**, 925-941. doi:10.1016/j.mod.2009.08.004
- Dong, B., Deng, W. and Jiang, D. (2011). Distinct cytoskeleton populations and extensive crosstalk control *Ciona* notochord tubulogenesis. *Development* **138**, 1631-1641. doi:10.1242/dev.057208
- Dosch, R. and Niehrs, C. (2000). Requirement for anti-dorsalizing morphogenetic protein in organizer patterning. *Mech. Dev.* **90**, 195-203. doi:10.1016/S0925-4773(99)00245-2
- Esterberg, R., Delalande, J.-M. and Fritz, A. (2008). Tailbud-derived *Bmp4* drives proliferation and inhibits maturation of zebrafish chordamesoderm. *Development* **135**, 3891-3901. doi:10.1242/dev.029264

- Gaviño, M. A. and Reddien, P. W. (2011). A Bmp/Admp regulatory circuit controls maintenance and regeneration of dorsal-ventral polarity in planarians. *Curr. Biol.* **21**, 294-299. doi:10.1016/j.cub.2011.01.017
- Gonzalez-Gobartt, E., Blanco-Ameijeiras, J., Usieto, S., Allio, G., Benazeraf, B. and Martí, E. (2021). Cell intercalation driven by SMAD3 underlies secondary neural tube formation. *Dev. Cell* **56**, 1147-1163.e6. doi:10.1016/j.devcel.2021.03.023
- Hara, Y., Nagayama, K., Yamamoto, T. S., Matsumoto, T., Suzuki, M. and Ueno, N. (2013). Directional migration of leading-edge mesoderm generates physical forces: Implication in *Xenopus* notochord formation during gastrulation. *Dev. Biol.* **382**, 482-495. doi:10.1016/j.ydbio.2013.07.023
- Hotta, K., Mitsuhara, K., Takahashi, H., Inaba, K., Oka, K., Gojobori, T. and Ikeo, K. (2007). A web-based interactive developmental table for the ascidian *Ciona intestinalis*, including 3D real-image embryo reconstructions: I. From fertilized egg to hatching larva. *Dev. Dyn.* **236**, 1790-1805. doi:10.1002/dvdy.21188
- Hotta, K., Dauga, D. and Manni, L. (2020). The ontology of the anatomy and development of the solitary ascidian *Ciona*: the swimming larva and its metamorphosis. *Sci. Rep.* **10**, 17916. doi:10.1038/s41598-020-73544-9
- Imai, K. S., Levine, M., Satoh, N. and Satou, Y. (2006). Regulatory blueprint for a chordate embryo. *Science (80-)* **312**, 1183-1187. doi:10.1126/science.1123404
- Imai, K. S., Daido, Y., Kusakabe, T. G. and Satou, Y. (2012). Cis-acting transcriptional repression establishes a sharp boundary in chordate embryos. *Science (80-)* **337**, 964-967. doi:10.1126/science.1222488
- Klaus, S. (1983). The evolution of patterning mechanisms: gleanings from insect embryogenesis and spermatogenesis. In *Development and Evolution* (ed. B. C. Goodwin and N. W. Holder), pp. 137-159. Cambridge University Press.
- Konstantinidis, G., Moustakas, A. and Stouraras, C. (2011). Regulation of myosin light chain function by BMP signaling controls actin cytoskeleton remodeling. *Cell. Physiol. Biochem.* **28**, 1031-1044. doi:10.1159/000335790
- Kumano, G., Ezal, C. and Smith, W. C. (2006). ADMP2 is essential for primitive blood and heart development in *Xenopus*. *Dev. Biol.* **299**, 411-423. doi:10.1016/j.ydbio.2006.08.010
- Lowe, C. J., Terasaki, M., Wu, M., Freeman, R. M., Jr, Runft, L., Kwan, K., Haigo, S., Aronowicz, J., Lander, E., Gruber, C. et al. (2006). Dorsoventral patterning in hemichordates: insights into early chordate evolution. *PLoS Biol.* **4**, e291. doi:10.1371/journal.pbio.0040291
- Lu, Q., Bhattachan, P. and Dong, B. (2019). Ascidian notochord elongation. *Dev. Biol.* **448**, 147-153. doi:10.1016/j.ydbio.2018.11.009
- Lu, Q., Gao, Y., Fu, Y., Peng, H., Shi, W., Li, B., Lv, Z., Feng, X.-Q. and Dong, B. (2020). *Ciona* embryonic tail bending is driven by asymmetrical notochord contractility and coordinated by epithelial proliferation. *Development* **147**, dev185868. doi:10.1242/dev.185868
- Matsumura, K. D., Nakamura, M. J., Koizumi, W. C., Hotta, K. and Oka, K. (2020). Different strategies for tissue scaling in dwarf tailbud embryos revealed by single-cell analysis. *Dev. Biol.* **460**, 215-223. doi:10.1016/j.ydbio.2020.01.008
- Mizotani, Y., Suzuki, M., Hotta, K., Watanabe, H., Shiba, K., Inaba, K., Tashiro, E., Oka, K. and Imoto, M. (2018). 14-3-3 $\epsilon$  directs the pulsatile transport of basal factors toward the apical domain for lumen growth in tubulogenesis. *Proc. Natl. Acad. Sci. USA* **115**, E8873-E8881. doi:10.1073/pnas.1808756115
- Miyamoto, D. M. and Crowther, R. J. (1985). Formation of the notochord in living ascidian embryos. *J. Embryol. Exp. Morphol.* **86**, 1-17. doi:10.1242/dev.86.1.1
- Munro, E. M. and Odell, G. (2002). Morphogenetic pattern formation during ascidian notochord formation is regulative and highly robust. *Development* **129**, 1-12. doi:10.1242/dev.129.1.1
- Nakamura, M. J., Terai, J., Okubo, R., Hotta, K. and Oka, K. (2012). Three-dimensional anatomy of the *Ciona intestinalis* tailbud embryo at single-cell resolution. *Dev. Biol.* **372**, 274-284. doi:10.1016/j.ydbio.2012.09.007
- Pasini, A., Amiel, A., Rothbacher, U., Roue, A., Lemaire, P. and Darras, S. (2006). Formation of the ascidian epidermal sensory neurons: insights into the origin of the chordate peripheral nervous system. *PLoS Biol.* **4**, e225. doi:10.1371/journal.pbio.0040225
- Richardson, M. K., Hanken, J., Gooneratne, M. L., Pieau, C., Raynaud, A., Selwood, L. and Wright, G. M. (1997). There is no highly conserved embryonic stage in the vertebrates: implications for current theories of evolution and development. *Anat. Embryol.* **196**, 91-106. doi:10.1007/s004290050082
- Roue, A. and Darras, S. (2016). Msxb is a core component of the genetic circuitry specifying the dorsal and ventral neurogenic midlines in the ascidian embryo. *Dev. Biol.* **409**, 277-287. doi:10.1016/j.ydbio.2015.11.009
- Sehring, I. M., Dong, B., Denker, E., Bhattachan, P., Deng, W., Mathiesen, B. T. and Jiang, D. (2014). An equatorial contractile mechanism drives cell elongation but not cell division. *PLoS Biol.* **12**, e1001781. doi:10.1371/journal.pbio.1001781
- Smith, H. M., Khairallah, S. M., Nguyen, A. H., Newman-Smith, E. and Smith, W. C. (2021). Misregulation of cell adhesion molecules in the *Ciona* neural tube closure mutant *bugeye*. *Dev. Biol.* **480**, 14-24. doi:10.1016/j.ydbio.2021.08.006
- Spemann, H. (1987). Embryonic Induction. *Am. Zool.* **27**, 575-579. doi:10.1093/icb/27.2.575
- Ubisch, V. L. V. (1939). KEIMBLATTCHIMÄRENFORSCHUNG AN SEEIGELLARVEN. *Biol. Rev.* **14**, 88-103. doi:10.1111/j.1469-185X.1939.tb00926.x
- von der Hardt, S., Bakkens, J., Inbal, A., Carvalho, L., Solnica-Krezel, L., Heisenberg, C.-P. and Hammerschmidt, M. (2007). The Bmp gradient of the zebrafish gastrula guides migrating lateral cells by regulating cell-cell adhesion. *Curr. Biol.* **17**, 475-487. doi:10.1016/j.cub.2007.02.013
- Waki, K., Imai, K. S. and Satou, Y. (2015). Genetic pathways for differentiation of the peripheral nervous system in ascidians. *Nat. Commun.* **6**, 8719. doi:10.1038/ncomms9719
- Willot, V., Mathieu, J., Lu, Y., Schmid, B., Sidi, S., Yan, Y.-L., Postlethwait, J. H., Mullins, M., Rosa, F., Peyri eras, N. et al. (2002). Cooperative action of ADMP- and BMP-mediated pathways in regulating cell fates in the zebrafish gastrula. *Dev. Biol.* **241**, 59-78. doi:10.1006/dbio.2001.0494
- Zhou, J., Pal, S., Maiti, S. and Davidson, L. A. (2015). Force production and mechanical accommodation during convergent extension. *Development* **142**, 692-701. doi:10.1242/dev.116533